Journal of Sound and Vibration (1997) **207**(3), 319–334

ON THE ANALYSIS OF VISCOELASTIC MATERIALS FOR ACTIVE CONSTRAINED LAYER DAMPING TREATMENTS

W. H. Liao and K. W. Wang

Structural Dynamics and Controls Research Laboratory, Mechanical Engineering Department, The Pennsylvania State University, University Park, PA 16802, *U.S.A.*

(*Received* 10 *May* 1996, *and in final form* 30 *April* 1997)

This paper is concerned with the investigations of viscoelastic material (VEM) effects on active constrained layer (ACL) based structures. Specific interests are on how the VEM parameters will influence the passive damping ability, the active action authority, and their combined effect in an ACL configuration. Using a beam example, the study has identified the VEM parameter regions that will provide the best active–passive hybrid actions. The results of this research can be used to develop guidelines to synthesize ACL structures that will outperform both the purely passive and active systems.

1. BACKGROUND

Active constrained layer (ACL) damping treatments generally consist of a piece of viscoelastic damping material (VEM) sandwiched between an active piezoelectric layer and the host structure. Such systems have been studied by various researchers [1–18]. It has been recognized that the active piezoelectric action in an ACL configuration will enhance the viscoelastic layer damping ability by increasing its shear angle during operation [6]. That is, the ACL can enhance the system damping when compared to a structure with traditional passive constrained layers (PCL). On the other hand, Van Nostrand [13] mentioned that the active actions will be degraded by the passive constrained layer. Bailey *et al*. [2] also stated that it is more effective to apply the piezoelectric materials directly on the structure (purely active case without the viscoelastic layer). Liao and Wang [18] recently illustrated that the viscoelastic layer will reduce the direct control authorities from the active source to the host structure, due to the reduction of transmissibility. Therefore, under some conditions, the ACL configuration could require more control effort while achieving less vibration reduction when compared to a purely active system (zero VEM thickness).

2. PROBLEM STATEMENT AND OBJECTIVE

From the above discussion, one can conclude that the overall performance of the ACL treatment, comparing it to a purely active configuration, depends on the combined effect of two factors. That is, (1) how much passive damping increment and (2) how much active action reduction are caused by adding the viscoelastic layer. The significance of this combined effect is of course very much dependent on the VEM properties. Therefore, to synthesize an ACL-based structure that can outperform both the purely passive and active systems, a thorough analysis on how the viscoelastic materials will influence the passive

0022–460X/97/430319 + 16 $25.00/0/sv971106

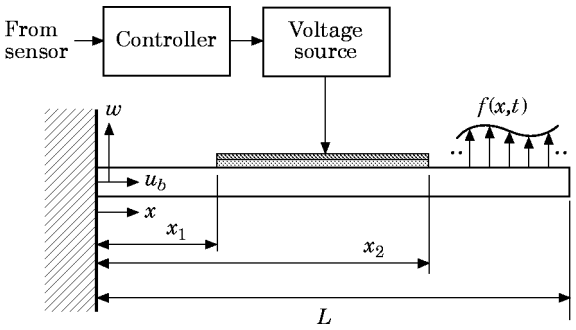

Figure 1. Cantilever beam with partially covered active constrained layer actuator: ▧, piezoelectric layer; □, viscoelastic layer.

damping and active action authority is needed. This effort will provide more understanding and physical insight to the problem, and further provide guidelines to ACL designers. Despite its importance, such a task had yet to be done. The goal of this research is to perform such an analysis and identify the important VEM parameters that will affect the aforementioned two factors, the passive damping ability and the active control authority, and their combined effects on structural controls.

3. SYSTEM DESCRIPTION

For the purpose of discussion, a cantilever beam with a partially covered active constrained layer is used to illustrate the concept (Figure 1). The piezoelectric cover sheet is connected to an external voltage source as the control input.

A finite element model has been developed for the system based on the following assumptions: (1) The rotatory inertia is negligible. The shear deformations in the piezoelectric layer and the beam are negligible. (2) The transverse displacement $w(x, t)$ is assumed to be the same for all layers. (3) Young's modulus of the VEM is negligible compared to those of the elastic and piezoelectric materials. (4) Linear theories of elasticity, viscoelasticity, and piezoelectricity are used. (5) There is perfect continuity at the interfaces, and no slip occurs between the layers. (6) The applied voltage is assumed uniform along the beam. (7) The density and thickness are uniform over the beam.

3.1. KINEMATICS RELATIONSHIPS

The geometry and deformation of the sandwich beam is shown in Figure 2. Let the axial displacements of the neutral axis of the piezoelectric layer, the VEM, and the beam be u_c, u_s, and u_b, respectively. The subscripts c, s, and b refer to the piezoelectric constraining layer, the viscoelastic shear layer (VEM), and the beam, respectively. Here, w denotes the

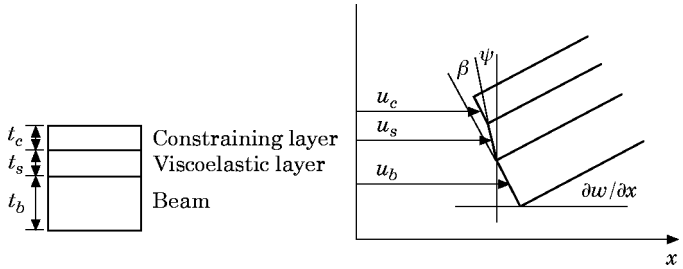

Figure 2. The geometry and deformation of a sandwich beam.

transverse displacement. A full list of symbols appears in the Appendix. From Figure 2, the shear strain β of the VEM is

$$\beta = \partial w/\partial x - \psi, \tag{1}$$

where ψ is the rotational angle of the VEM layer. For perfect bonding conditions, one can further derive the kinematics relations

$$u_s = u_b - (t_b/2)\,(\partial w/\partial x) - (t_s/2)\psi, \qquad u_c = u_b - (t_b + t_c)/2\,(\partial w/\partial x) - t_s\psi. \tag{2, 3}$$

3.2. ENERGY OF BEAM WITH ACL TREATMENTS

For one-dimensional structures with uni-axial loading, the constitutive equation of the piezoelectric materials [19] can be written as

$$\begin{bmatrix} \tau \\ E \end{bmatrix} = \begin{bmatrix} C_{11}^D & -h_{31} \\ -h_{31} & \beta_{33}^S \end{bmatrix} \begin{bmatrix} \varepsilon \\ D \end{bmatrix}, \tag{4}$$

where D is the electrical displacement (charge/area in the beam vertical direction), E is the electrical field (voltage/length along the vertical direction), ε is the mechanical strain in the x direction, and τ is the mechanical stress in the x direction. C_{11}^D is the elastic stiffness, β_{33}^S is the dielectric constant, and h_{31} is the piezoelectric constant. Based on the above constitutive equation, and assuming D is constant along the piezoelectric layer thickness for thin materials, one can derive the potential energies of the piezoelectric layer and the beam to be

$$E_P^c = \frac{1}{2}\int_{V_c} (\tau\varepsilon + ED)\,\mathrm{d}V = \frac{1}{2}\int_0^L \left[C_{11}^D A_c \left(\frac{\partial u_c}{\partial x}\right)^2 + C_{11}^D I_c \left(\frac{\partial^2 w}{\partial x^2}\right)^2 \right.$$

$$\left. - 2A_c h_{31} D\left(\frac{\partial u_c}{\partial x}\right) + A_c \beta_{33}^S D^2 \right] [\mathrm{H}(x - x_1) - \mathrm{H}(x - x_2)]\,\mathrm{d}x, \tag{5}$$

$$E_P^b = \frac{1}{2}\int_0^L \left[E_b A_b \left(\frac{\partial u_b}{\partial x}\right)^2 + E_b I_b \left(\frac{\partial^2 w}{\partial x^2}\right)^2 \right] \mathrm{d}x, \tag{6}$$

where I_c and I_b are the moments of inertia about the neutral axis of the piezoelectric layer and the beam, respectively. H is the Heaviside's unit function. The other parameters are defined in the nomenclature.

The kinetic energies of the beam, the VEM layer, and the cover sheet (T_b, T_s, T_c respectively) are represented as

$$T_b = \frac{1}{2}\int_0^L \rho_b A_b \left[\left(\frac{\partial u_b}{\partial t}\right)^2 + \left(\frac{\partial w}{\partial t}\right)^2 \right] \mathrm{d}x, \tag{7}$$

$$T_s = \frac{1}{2}\int_0^L \left[\rho_s A_s \left[\left(\frac{\partial u_s}{\partial t}\right)^2 + \left(\frac{\partial w}{\partial t}\right)^2 \right] \right] [\mathrm{H}(x - x_1) - \mathrm{H}(x - x_2)]\,\mathrm{d}x, \tag{8}$$

$$T_c = \frac{1}{2}\int_0^L \left[\rho_c A_c \left[\left(\frac{\partial u_c}{\partial t}\right)^2 + \left(\frac{\partial w}{\partial t}\right)^2 \right] \right] [\mathrm{H}(x - x_1) - \mathrm{H}(x - x_2)]\,\mathrm{d}x. \tag{9}$$

All parameters used in the above equations are defined in the nomenclature.

3.3. VIRTUAL WORK

For one-dimensional systems, the constitutive equation for viscoelastic materials can be represented in the Stieltjes integral form [20]

$$\tau(x, t) = G \circ \beta \equiv \int_{-\infty}^{t} G(t-\tau)\frac{\partial \beta}{\partial \tau}(x, \tau)\,\mathrm{d}\tau, \tag{10}$$

where $G(t)$ is the relaxation function of VEM (the stress response to a unit-step strain input). This stress relaxation represents energy loss from the material, hence damping. The virtual work done by the viscoelastic layer is therefore

$$\delta W_s = -\int_0^L A_s (G \circ \beta)\,\delta\beta[\mathrm{H}(x-x_1) - \mathrm{H}(x-x_2)]\,\mathrm{d}x. \tag{11}$$

The virtual work done by the applied voltage is

$$\delta W_c = \int_0^L bV(t)\,\delta D[\mathrm{H}(x-x_1) - \mathrm{H}(x-x_2)]\,\mathrm{d}x. \tag{12}$$

The virtual work done by the external disturbance force is

$$\delta W_d = \int_0^L f(x, t)\,\delta w(x, t)\,\mathrm{d}x. \tag{13}$$

3.4. FINITE ELEMENT MODEL

The finite element method (FEM) [21] is used to convert energy and work equations (5–13) into forms of global nodal displacements through matrix assembly of the elements. The local shape functions are chosen to be cubic polynomial in x (for transverse displacement w) and linear polynomial in x (for axial displacement u_b and shear angle β). During the discretization process, the Golla–Hughes–McTavish (GHM) method [22, 23] is employed to analyze the Stieltjes integral in the time domain [17, 18]. The detailed development of the model can be found in reference [24]. The total number of elements used in the analysis presented in this paper is ten. This includes a combination of two (left plain beam region), five (ACL sandwich beam region), and three (right plain beam region), as illustrated in Figure 3. The elements are of equal length within each region.

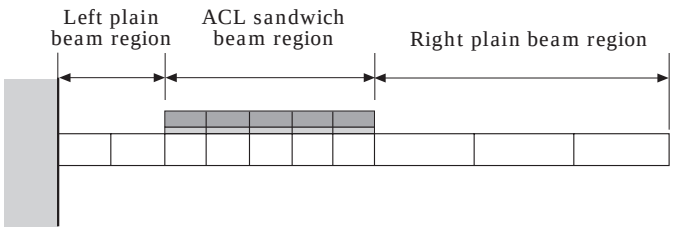

Figure 3. Finite element model of beam with partially covered ACL (constraining layer identification as in Figure 1).

Using Hamilton's principle, one can construct

$$\int_{t_1}^{t_2} [\delta T_b + \delta T_s + \delta T_c - \delta E_P^b - \delta E_P^c + \delta W_s + \delta W_c + \delta W_d] \, \mathrm{d}t = 0. \tag{14}$$

With the kinematics relations (1–3), one can derive the discretized *time-domain* model:

$$\mathbf{M}\ddot{\mathbf{q}} + C\dot{\mathbf{q}} + \mathbf{K}\mathbf{q} = \mathbf{f}_c + \mathbf{f}_d, \tag{15}$$

where $\mathbf{q}$, $\dot{\mathbf{q}}$, and $\ddot{\mathbf{q}}$ are vectors of nodal displacement, velocity, and acceleration. $\mathbf{M}$, $\mathbf{C}$, and $\mathbf{K}$ are the mass, damping, and stiffness matrices which are symmetric. In addition, $\mathbf{f}_c$ and $\mathbf{f}_d$ are vectors representing the control and disturbance forces, respectively. In the above formulation, the internal structural damping is also included via Rayleigh damping, which is of the form $\mathbf{C}_b = \hat{a}\mathbf{M}_b + \hat{b}\mathbf{K}_b$. Here, $\mathbf{M}_b$ and $\mathbf{K}_b$ are submatrices of $\mathbf{M}$ and $\mathbf{K}$, respectively, from which the parts corresponding to the GHM dissipation co-ordinates are excluded. Constants $\hat{a}$ and $\hat{b}$ can be determined from experiments [21].

The discretized equation can be placed in the standard state-space form:

$$\dot{\mathbf{x}} = \mathbf{A}\mathbf{x} + \mathbf{B}\mathbf{u} + \hat{\mathbf{B}}\mathbf{u}_d, \qquad \mathbf{y} = \mathbf{C}_o\mathbf{x}, \tag{16, 17}$$

where $\mathbf{A}$ is the system matrix, $\mathbf{B}$ is the control matrix, $\hat{\mathbf{B}}$ is the disturbance matrix, $\mathbf{C}_o$ is the output matrix, and $\mathbf{u}_d$ is the disturbance input vector. The state vector $\mathbf{x}$ and control input $\mathbf{u}$ are defined by

$$\mathbf{x} = [\mathbf{q}^{\mathrm{T}} \quad \dot{\mathbf{q}}^{\mathrm{T}}]^{\mathrm{T}}, \qquad \mathbf{u} = V(t). \tag{18, 19}$$

By removing the VEM layer parameters, a model for the purely active configuration with similar procedures has also been derived [24].

3.5. EXPERIMENTAL VALIDATION

To validate the finite element models described in the previous section, laboratory experiments have been performed. Figure 4 illustrates the experimental setup. Two cantilever beam specimens are constructed: one is an ACL-based structure, the other is a purely active configuration (direct application of the piezoelectric layer on the beam without the VEM). Other than the VEM layer, both specimens have the same materials and dimensions. The actuator layers are bonded to the aluminium beams (261·6 mm × 12·7 mm × 2·286 mm) at 27 mm from the fixed end. The piezoelectric cover sheet (101·6 mm × 12·7 mm × 0·762 mm) is made of PZT ceramics (PKI 502). A well-known viscoelastic material, 3M ISD 112, is used for the damping layer (101·6 mm × 12·7 mm × 0·254 mm).

To test their open loop frequency responses, the beams are excited by the actuators with white noise inputs. The beam vibrations are measured using a non-contact displacement

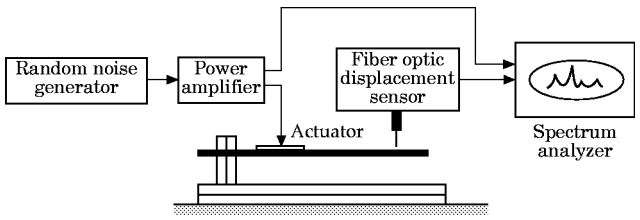

Figure 4. Schematic of experimental setup.

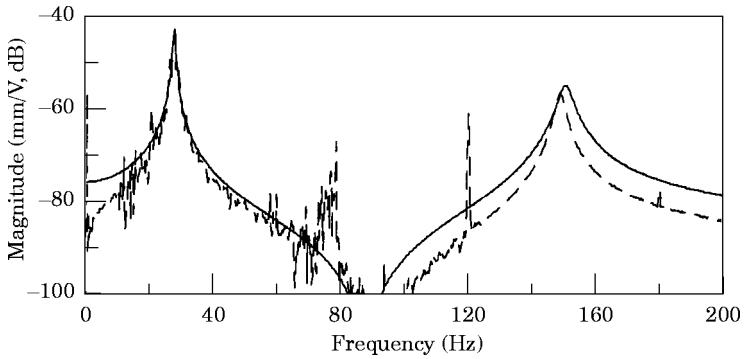

Figure 5. Frequency response of ACL system: ——, FEM; — —, experiment.

probe (PHILTEC, Model A88N1) located 2 mm from the free end, and processed through a signal analyzer (HP 35665A).

Figure 5 shows the ACL-based structure's frequency response function (measured displacement over input voltage). The frequency response of the purely active configuration is illustrated in Figure 6. Analytical results obtained from the finite element models are also shown in the figures. The system parameters used in this study are summarized in Table 1. It is illustrated that the analytical predictions match the experimental data closely. These experiments demonstrate the validity of the models.

4. ANALYSIS AND DISCUSSIONS

To evaluate the active–passive hybrid actions, an analysis has been carried out on the beam structure model described in the previous section. The system parameter values used are given in Table 1 unless stated otherwise. In the following sections, the GHM parameters will first be related to the physical properties of the viscoelastic materials, and then the significance of these variables on the system's passive damping ability, active action authority, and their combined effect discussed.

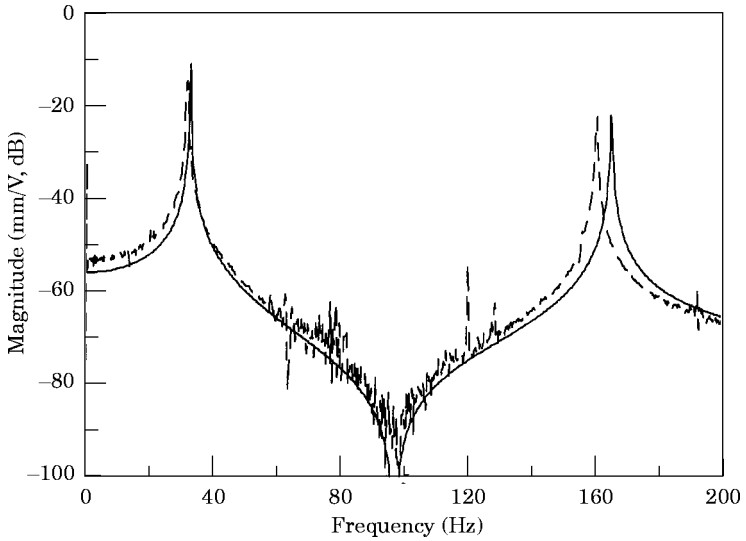

Figure 6. Frequency response of purely active system: Key as for Figure 5.

TABLE 1

System parameters

$\hat{a}$	0·64	R	1	κ (Pa)	5×10^5
b (mm)	12·7	t_b (mm)	2·286	β_{33}^s (V²/N)	$3{\cdot}94 \times 10^7$
$\hat{b}$	$1{\cdot}2 \times 10^{-6}$	t_c (mm)	0·762	ρ_b (kg/m³)	2700
C_{11}^D (N/m²)	$7{\cdot}40 \times 10^{10}$	t_s (mm)	0·25	ρ_c (kg/m³)	7600
E_b (N/m²)	$7{\cdot}1 \times 10^{10}$	x_1 (mm)	27	ρ_s (kg/m³)	1250
h_{31} (V/m)	$-6{\cdot}73 \times 10^8$	x_2 (mm)	128·6	$\hat{\omega}$ (rad/s)	10 000
L (mm)	261·6	α	6·0	$\hat{\zeta}$	4·0

4.1. A DISCUSSION ON GHM PARAMETERS

The GHM method [22, 23] represents the material modulus function as a series of mini-oscillator terms in the Laplace domain:

$$s\tilde{G}(\mathbf{s}) = \kappa\left[1 + \sum_{r=1}^{n} \alpha_r \frac{s^2 + 2\hat{\zeta}_r\hat{\omega}_r s}{s^2 + 2\hat{\zeta}_r\hat{\omega}_r s + \hat{\omega}_r^2}\right]. \tag{20}$$

The factor κ corresponds to the equilibrium value of the modulus—the final value of the relaxation function $G(t)$. Each mini-oscillator term is a second order rational function involving three positive constants $\{\alpha_r, \hat{\omega}_r, \hat{\zeta}_r\}$. These constants govern the shape of the modulus function over the complex **s**-domain.

Consider a single-term GHM expression:

$$s\tilde{G}(\mathbf{s}) = \kappa\left[1 + \alpha \frac{s^2 + 2\hat{\zeta}\hat{\omega}s}{s^2 + 2\hat{\zeta}\hat{\omega}s + \hat{\omega}^2}\right]. \tag{21}$$

This modulus function, when evaluated along the imaginary axis of the **s**-plane, yields the complex modulus

$$G^*(\omega) \equiv \mathrm{i}\omega\tilde{G}(\mathrm{i}\omega) = G_1(1 + \mathrm{i}\eta). \tag{22}$$

With equations (21) and (22), the shear (storage) modulus $G_1(\omega)$ and material loss factor $\eta(\omega)$ can be derived as

$$G_1(\omega) = \kappa\left[1 + \alpha \frac{\omega^4 + (4\hat{\zeta}^2 - 1)\hat{\omega}^2\omega^2}{\omega^4 + 2(2\hat{\zeta}^2 - 1)\hat{\omega}^2\omega^2 + \hat{\omega}^4}\right], \tag{23}$$

$$\eta(\omega) = \alpha \frac{2\hat{\zeta}\hat{\omega}^3\omega}{(1 + \alpha)\omega^4 + [4(1 + \alpha)\hat{\zeta}^2 - 1]\hat{\omega}^2\omega^2 + \hat{\omega}^4}. \tag{24}$$

Figures 7 and 8 illustrate the relations among the shear modulus, loss factor and the GHM parameters. Figure 7 shows the shear modulus for different κ over the frequency range from 1 to 10 000 rad/s. Note that the shear modulus is proportional to κ. Figure 8 shows the effects of α on the loss factor and shear modulus. It is interesting to note that larger α corresponds to larger loss factor and shear modulus, while the effect changes with frequency.

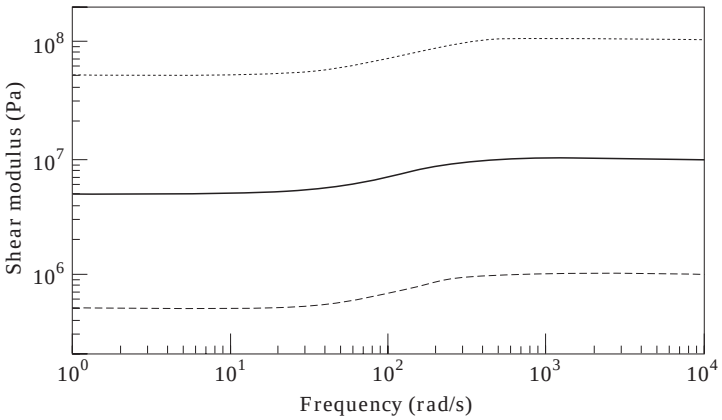

Figure 7. The shear modulus for different κ ($\alpha = 1, \hat{\omega} = 1000$ rad/s): k values; · · · · · , 5×10^7; ——, 5×10^6; ----, 5×10^5 Pa.

4.2. PERFORMANCE (J_1) AND CONTROL EFFORT (J_2) INDEXES

For broadband excitation considerations, one can assume the external disturbance to be a zero-mean white noise process:

$$\mathrm{E}[\mathbf{u}_d(t)] = 0, \qquad \mathrm{E}[\mathbf{u}_d(t)\mathbf{u}_d^{\mathrm{T}}(\tau)] = \mathbf{U}_{\mathbf{d}}(t)\,\delta(t-\tau). \tag{25, 26}$$

The system response will consist of a state vector with zero mean and a variance given by the solution ($\mathbf{P_l}$) to the Lyapunov equation

$$\mathbf{A}\mathbf{P_l} + \mathbf{P_l}\mathbf{A}^{\mathrm{T}} + \hat{\mathbf{B}}\mathbf{U_d}\hat{\mathbf{B}}^{\mathrm{T}} = 0, \tag{27}$$

where

$$\mathbf{P_l} = \mathrm{E}[\mathbf{x}(t)\mathbf{x}^{\mathrm{T}}(t)]. \tag{28}$$

The output covariance matrix can be written as

$$W = \mathrm{E}[\mathbf{y}\mathbf{y}^{\mathrm{T}}] = \mathrm{E}\{[\mathbf{C}_o\,\mathbf{x}]\,[\mathbf{C}_o\,\mathbf{x}]^{\mathrm{T}}\} = \mathrm{E}\{\mathbf{C}_o\,\mathbf{x}\mathbf{x}^{\mathrm{T}}\mathbf{C}_o^{\mathrm{T}}\} = \mathbf{C}_o\,\mathrm{E}[\mathbf{x}\mathbf{x}^{\mathrm{T}}]\mathbf{C}_o^{\mathrm{T}} = \mathbf{C}_o\,\mathbf{P_l}\mathbf{C}_o^{\mathrm{T}}. \tag{29}$$

In this research, covariance response to white noise is observed. A random disturbance with variance ($2{\cdot}5 \times 10^{-5}$) is applied to the beam at the free end and the output $\mathbf{y}$ is chosen to reflect the beam tip displacement.

To investigate the system characteristics, one defines the standard deviations of the output vibration amplitude and required voltage as J_1 and J_2, respectively. Here, J_1 is an index representing the vibration suppression performance (the less J_1, the better the performance) and J_2 is an index representing the required control effort.

4.3. PASSIVE DAMPING ABILITY

For the purely passive case ($V(t) = 0$), define $J_1 = J_{1P}$. One then defines J_{1P0} to be the J_{1P} value for a case without VEM damping (by removing the GHM dissipation co-ordinates, but still keeping the VEM stiffness modulus) and J_{1Pd} to be the J_{1P} value with VEM damping. That is, J_{1P0} and J_{1Pd} are obtained with the same system static stiffness for given parameters. One then defines an index to quantify the VEM passive damping ability:

$$I_p = [(J_{1P0} - J_{1Pd})/J_{1P0}]100. \tag{30}$$

Here, $(J_{1P0} - J_{1Pd})$ can be viewed as vibration amplitude reduction due to contributions mainly from the VEM damping. The I_p values versus κ and α are shown in Figure 9. For

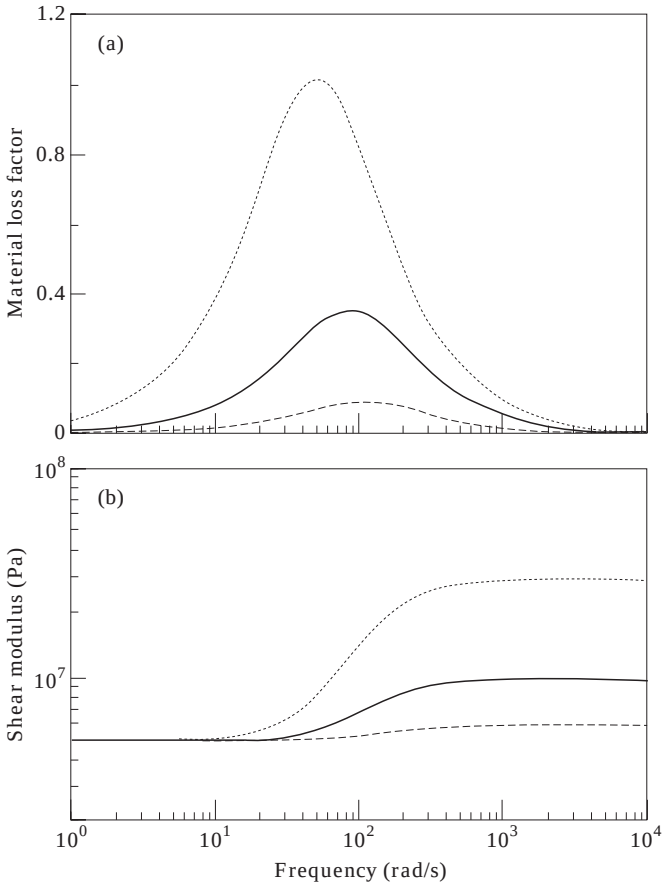

Figure 8. (a) The material loss factor for different α ($\dot{\omega} = 1000$ rad/s), (b) the shear modulus for different α ($\kappa = 5 \times 10^6$ Pa, $\dot{\omega} = 1000$ rad/s): α values; · · · · ·, 5; ——, 1·0; ----, 0·2.

a specific α, there exists an optimal κ value for maximum I_p. For a specific κ, the I_p increases with increasing α. The major reason is that larger α corresponds to larger loss factor of the VEM and thus provides larger system damping.

The I_p values versus κ and t_s are shown in Figure 10. Given a specific t_s, there again exists an optimal κ value corresponding to a maximum I_p. For a specific κ, the I_p first

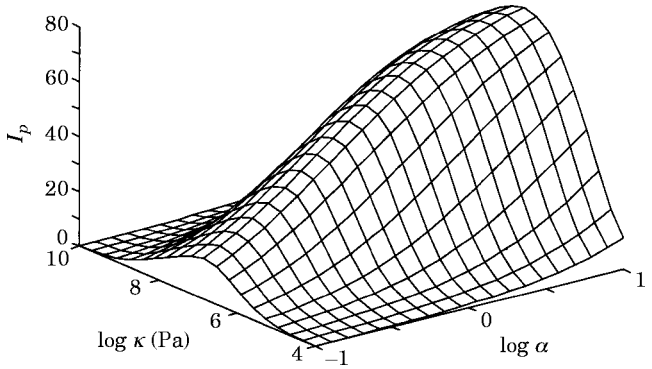

Figure 9. I_p versus κ and α ($t_s = 0{\cdot}25$ mm)

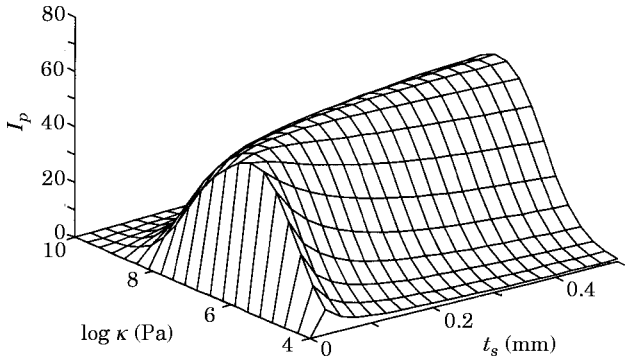

Figure 10. I_p versus κ and t_s ($\alpha = 1$).

increases as t_s increases from zero (without VEM layer), but will start to decrease with t_s for sufficiently large t_s. In other words, for given material properties, there exists an optimal VEM thickness corresponding to the maximum passive system damping. These observations are consistent with those in previous PCL studies [25, 26].

4.4. ACTIVE ACTION AUTHORITY

To examine the active action authority of various configurations, the structure is statically deformed by the actuator with DC voltage input. The beam deflection at the free end is further transferred to an equivalent point load (transmitted force) by multiplying it by the equivalent beam stiffness at the tip. Given the same input voltage, larger transmitted force indicates higher authority of the active action. The transmitted force per input voltage is then normalized with respect to that of the purely active system, which is defined to be I_a. Here, I_a is an index to quantify the active action authority, which is expressed as

$$I_a = (X_V/X_F)/(X_V/X_F)_{PA}, \tag{31}$$

where X_V is the static beam deflection at the free end when unit DC voltage is applied to the actuator, and X_F is the beam tip deflection when a unit static force in the transverse direction is applied to the beam at the free end. The subscript PA refers to the purely active system.

The I_a values for different κ are plotted against t_s in Figure 11. It should be noted that the purely active system is the case with $t_s = 0$. From the figure, one sees that I_a increases with increasing κ for the same t_s (same offset). This shows that the VEM shear modulus (proportional to κ) is a key factor on the active action authority of the ACL configuration. It is also illustrated that the I_a value for typical κ's ($\kappa < 10^8$ Pa) reduces significantly as t_s increases from 0. This phenomenon indicates that the active action is degraded by the VEM layer. The reason is that the soft viscoelastic layer reduces the direct control authorities being transmitted (transmissibility) from the piezoelectric actuator to the host structure. For such cases, the active action authority decreases with increasing VEM thickness even though the offset (the distance between the neutral axis of the beam and that of the piezoelectric cover sheet) is increased. When κ is very large ($\kappa \geqslant 10^9$ Pa, beyond the value of typical VEMs), the active action authority can be higher than that of the purely active configuration ($t_s = 0$) due to the "offset" effects. The active action authority does not vary with α because only the static beam deflection is considered for I_a.

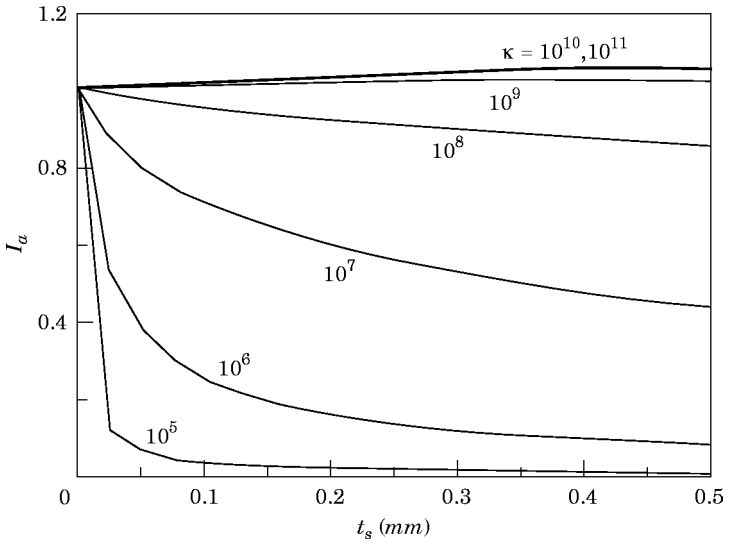

Figure 11. I_a versus t_s, with different κ.

4.5. CONTROL LAW DEVELOPMENT

The Popov–Belevitch–Hautus (PBH) rank tests [27] are applied to check the system' controllability characteristics. Using the parameters in Table 1, both the purely active and the ACL-based structures satisfy the conditions in the PBH tests. This implies both systems are controllable for the given configurations.

For the purpose of fair comparison among different cases, the optimal control theory [28, 29] is used to determine the active control gains. To examine the system response under broadband excitation, a stochastic regulator problem is formulated. The average cost is given as

$$J_S = \lim_{t_f \to \infty} \frac{1}{t_f} \mathrm{E}\left[\int_0^{t_f} (\mathbf{y}^{\mathrm{T}}\mathbf{Q}\mathbf{y} + \mathbf{u}^{\mathrm{T}}\mathbf{R}\mathbf{u})\, \mathrm{d}t\right]. \tag{32}$$

Here, E[] is the expectation operator, $\mathbf{Q}$ and $\mathbf{R}$ are the semi-positive-definite and positive-definite weighting matrices on the outputs and control inputs, respectively. Since one wants to focus on the actuator characteristics in this paper, full-state feedback is assumed. The control law is given by

$$\mathbf{u} = -\mathbf{K}_{\mathrm{c}}\mathbf{x} \tag{33}$$

with control gain $\mathbf{K}_{\mathrm{c}} = \mathbf{R}^{-1}\mathbf{B}^{\mathrm{T}}P$. Here, $\mathbf{P}$ satisfies the algebraic Riccati equation

$$\mathbf{A}^{\mathrm{T}}\mathbf{P} + \mathbf{P}\mathbf{A} - \mathbf{P}\mathbf{B}\mathbf{R}^{-1}\mathbf{B}^{\mathrm{T}}\mathbf{P} + \mathbf{C}_o^{\mathrm{T}}\mathbf{Q}\mathbf{C}_o = 0. \tag{34}$$

The closed-loop system thus becomes

$$\dot{\mathbf{x}} = (\mathbf{A} - \mathbf{B}\mathbf{K}_{\mathrm{c}})\mathbf{x} + \hat{\mathbf{B}}\mathbf{u}_d = \mathbf{A}_{\mathrm{cl}}\mathbf{x} + \hat{\mathbf{B}}\mathbf{u}_d. \tag{35}$$

4.6. ACTIVE–PASSIVE HYBRID ACTIONS

From the discussions in sections 4.3 and 4.4, one sees that the VEM parameters can have significant influence on both the passive damping ability and active action authority of the ACL treatments. The major interest now is to study the VEM parametric effect on the

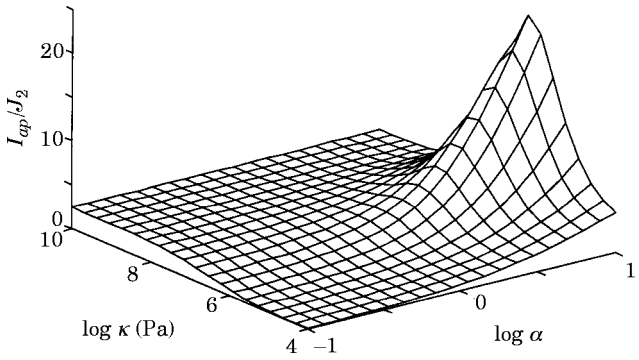

Figure 12. I_{ap}/J_2 versus κ and α for $Q = 10^9$ ($t_s = 0{\cdot}25$ mm).

overall system performance combining the active and passive actions. To investigate this, one defines an index I_{ap},

$$I_{ap} = [(J_{1P0} - J_1)/J_{1P0}]100. \tag{36}$$

Here, $(J_{1P0} - J_1)$ can be viewed as the vibration amplitude reduction due to contributions from the combined active–passive hybrid actions. (I_{ap}/J_2) thus represents the vibration suppression ability per control effort, which indicates the effectiveness or efficiency of the active–passive hybrid actions (closed loop system).

The I_{ap}/J_2 values versus κ and α for three different weightings are plotted in Figures 12–14. One sees that I_{ap}/J_2 decreases as Q (demand on vibration suppression capability) increases, given the same κ and α. With small or medium Q (indicating less demand on performance), the overall index I_{ap}/J_2 is affected by both the passive damping ability and active action transmissibility. Therefore, I_{ap}/J_2 has maximum values in the regions corresponding to large α and certain optimal κ (see Figures 12 and 13). With large Q (indicating high demand on performance), it is shown that the larger κ the better (Figure 14). This indicates that the passive damping ability from the VEM is not large enough to make any major contributions to the result. In other words, I_{ap}/J_2 is dominated by the active action effect such that the higher the transmissibility (active action authority) the better.

The I_{ap}/J_2 values versus κ and t_s for two different weightings are plotted in Figures 15 and 16. With smaller Q (Figures 15), the overall index I_{ap}/J_2 is dominated by both the passive damping and active action authority (transmissibility) effects, which has maximum

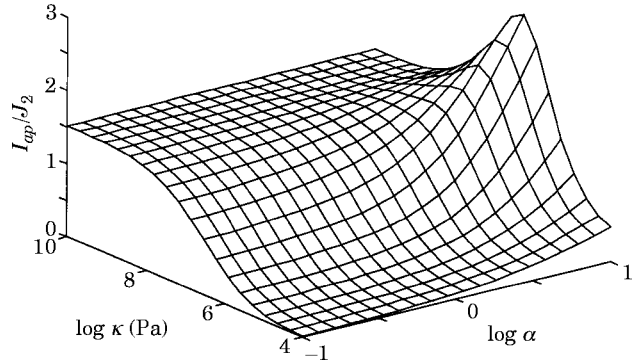

Figure 13. I_{ap}/J_2 versus κ and α for $Q = 10^{10}$ ($t_s = 0{\cdot}25$ mm).

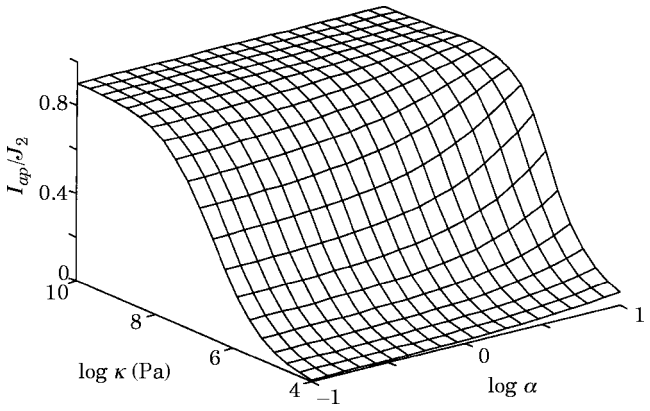

Figure 14. I_{ap}/J_2 versus κ and α for $Q = 10^{11}$ ($t_s = 0{\cdot}25$ mm).

values in the range corresponding to certain optimal κ and t_s values. It should be noted that the line corresponding to $t_s = 0$ represents the purely active case. One can see that the I_{ap}/J_2 in the optimal range is larger than the active case I_{ap}/J_2, which indicates that the ACL design could outperform the purely active structure. However, the ACL system could also be worse than the purely active case if one is not careful (the range in which the ACL I_{ap}/J_2 surface is lower than the zero VEM thickness line). On the other hand,

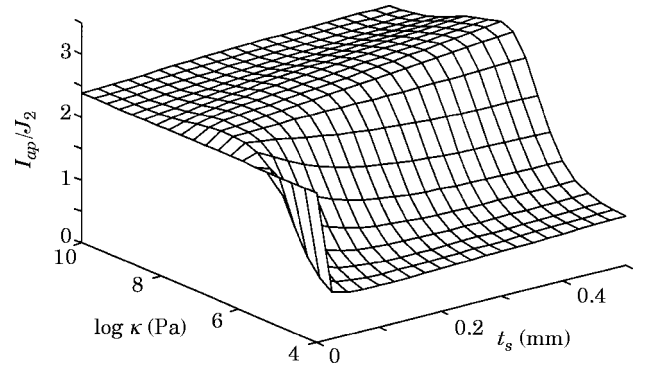

Figure 15. I_{ap}/J_2 versus κ and t_s for $Q = 10^9$ ($\alpha = 1$).

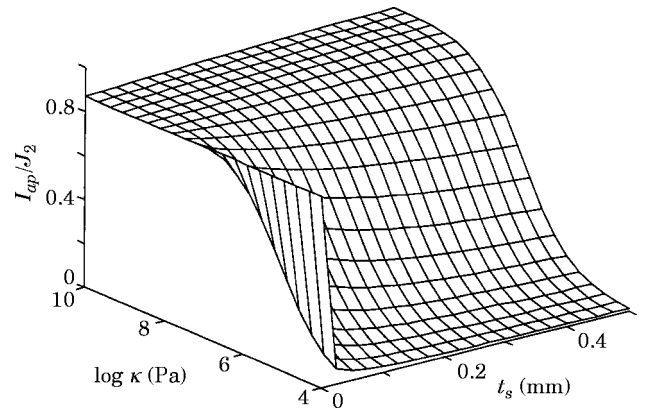

Figure 16. I_{ap}/J_2 versus κ and t_s for $Q = 10^{11}$ ($\alpha = 1$).

one needs significantly large κ to outperform the purely active case with higher Q (Figure 16). This is again because that the passive damping effect is not significant enough, and the results are dominated by the active action. Therefore, the transmissibility becomes the major issue.

4.7. SUMMARY

From the analysis presented in this paper, some guidelines for ACL designs are summarized in the following paragraphs.

(1) It is desirable to let the VEM loss factor (directly related to the α value) be as large as possible to obtain good passive damping abilities and active–passive hybrid actions in ACL designs.

(2) The VEM shear modulus can be categorized as having three regions: low, medium, and high. In the low shear modulus region (e.g., $\kappa < 10^5$ Pa in the given example), both the passive damping ability and active action authority (transmissibility) are low for the ACL structure, and therefore the overall performance of the active–passive hybrid system is poor. One should avoid using VEM in this region while designing ACL structures.

(3) To obtain large vibration reduction with high demand on performance (little concern of control effort), high active gains (high weighting on performance) are usually used. In such cases, one could select VEM with high shear modulus (e.g., 10^8 Pa $< \kappa$ in the given example) to achieve high transmissibility of the active actions. However, the differences between the ACL and the purely active configurations might not be very obvious (Figure 16). Another point worth noting is that when κ becomes too large, the passive VEM damping could become ineffective (Figure 9), and the ACL's fail-safe ability (which is a desirable feature of such active–passive hybrid structures) could be significantly reduced.

(4) To achieve good vibration reduction performance with significant constraints on control effort, the active gain values (weighting on performance) are usually limited. This is the best scenario for applying ACL, where the benefits of both the passive damping and active action could be obtained. In this case, one should choose the VEM shear modulus in the medium region (e.g., 10^5 Pa $< \kappa < 10^8$ Pa in the given example). Generally, this is the most useful region for ACL designs. Also in such designs, there exists an optimal VEM thickness which corresponds to the maximum hybrid active–passive actions in ACL systems. Usually, this optimal thickness value is small compared to those of the main structure and the piezoelectric layer, which makes such configurations quite achievable.

5. CONCLUSION

From the results presented in this paper, it is clear that several additional factors need to be considered in an ACL design versus a classical PCL design. These extra factors include the control gains and the VEM transmissibility. This study has identified the VEM parameter regions that will provide satisfactory transmissibility of the active actions, and have overall results outperforming both purely passive and active systems. While this investigation is helpful in setting up guidelines for ACL designers, it also illustrates that the VEM design space is more limited for ACL than PCL. Also, since VEM properties vary significantly with temperature and age, an original effective design with sufficient transmissibility could become much less effective as operating condition changes. Based on these arguments, it will be desirable if one can develop means to reduce the VEM effect on active action transmissibility, while retaining the passive damping ability in the ACL. This could increase the design space for VEM selections, and enhance the ACL's overall

active–passive combined performance and robustness. A new idea has recently been developed [24, 30, 31] for such purposes, which could be a good direction for future research.

ACKNOWLEDGMENT

This research is supported by the U.S. Army Research Office.

REFERENCES

1. J. M. Plump and J. E. Hubbard Jr. 1986 12*th International Congress on Acoustics*, D4-1, Toronto, Canada. Modeling of an active constrained layer damper.
2. T. Bailey, A. Gruzen and P. Madden 1988 AFAL-TR-88-038. RCS/Piezoelectric Distributed Actuator Study.
3. G. Agnes and K. Napolitano 1993 *Proceedings* 34*th AIAA/ASME/ASCE/AHS/ASC Structures*, *Structural Dynamics and Materials Conference*, 3499–3506. Active constrained layer viscoelastic damping.
4. A. Baz 1993 *Proceedings of Damping* 93 IBB 1–23. Active constrained layer damping.
5. A. Baz and J. Ro 1993 *Recent Developments in Stability*, *Vibration*, *and Control of Structural Systems*, ASME-AMD-167, 61–80. Partial treatment of flexible beams with active constrained layer damping.
6. A. Baz and J. Ro 1994 *Sound and Vibration*, 18–21. The concept and performance of active constrained layer damping treatments.
7. A. Baz and J. Ro 1994 *Proceedings of Conference on Smart Structures and Materials*, SPIE **2193**, 98–114. Performance characteristics of active constrained layer damping.
8. A. Baz and J. Ro 1995 *ASME Special* 50*th Anniversary Design Issue* **117**, 135–144. Optimum design and control of active constrained layer damping.
9. I. Y. Shen 1994 *ASME Journal of Vibration and Acoustics* **116**, 341–349. Hybrid damping through intelligent constrained layer treatments.
10. I. Y. Shen 1994 *Journal of Smart Materials and Structures* **3**, 59–70. Bending vibration control of composite and isotropic plates through intelligent constrained-layer treatments.
11. I. Y. Shen 1995 *Proceedings of the* 1995 *Design Engineering Technical Conferences*, ASME DE **84**-3, 149–160. Variational formulation, work-energy relation and damping mechanism of active constrained layer treatments.
12. I. Y. Shen 1996 *ASME Journal of Vibration and Acoustics* **118**, 70–77. Stability and controllability of Euler–Bernoulli beams with intelligent constrained layer treatments.
13. W. C. Van Nostrand 1994 *Ph.D. Dissertation*, *State University of New York at Buffalo*. Active constrained layer damping using PZT actuators.
14. W. C. Van Nostrand, G. Knowles and D. J. Inman 1993 *Dynamics and Control of Structures in Space* **II**, 667–681. Active constrained layer damping for micro-satellites.
15. W. C. Van Nostrand, G. Knowles and D. J. Inman 1994 *Proceedings of Conference on Smart Structures and Materials*, SPIE **2193**, 126–137. Finite element model for active constrained layer damping.
16. B. Azvine, G. R. Tomlinson and R. J. Wynne 1995 *Journal of Smart Materials and Structures*, **4**, 1–6. Use of active constrained layer damping for controlling resonant vibration.
17. M. J. Lam, W. R. Saunders and D. J. Inman 1995 *Proceedings of Conference on Smart Structures and Materials SPIE* **2445**, 86–97. Modeling active constrained layer damping using the Golla–Hughes–McTavish approach.
18. W. H. Liao and K. W. Wang 1995 *Proceedings of the* 1995 *Design Engineering Technical Conferences*, ASME DE **84**-3, 125–141. On the active–passive hybrid vibration control actions of structures with active constrained layer treatments.
19. ANSI-IEEE Std 176-1987. *IEEE Standard on Piezoelectricity*.
20. R. M. Christensen 1982 *Theory of Viscoelasticity*: *an Introduction*. New York: Academic Press; second edition.
21. K. J. Bathe 1996 *Finite Element Procedures*. Englewood Cliffs, New Jersey; Prentice-Hall.
22. D. F. Golla and P. C. Hughes 1985 *Journal of Applied Mechanics* **52**, 897–906. Dynamics of viscoelastic structures—a time domain, finite element formulation.
23. D. J. McTavish and P. C. Hughes 1993 *ASME Journal of Vibration and Acoustics* **115**, 103–110. Modeling of linear viscoelastic space structures.

24. W. H. Liao 1997 *Ph.D. Thesis*, *The Pennsylvania State University*. Active-passive hybrid structural control: an enhanced active constrained layer damping treatment with edge elements.
25. D. K. Rao 1978 *Journal of Mechanical Engineering Science* **20**, 271–282. Frequency and loss factors of sandwich beams under various boundary conditions.
26. A. Nashif, D. I. G. Jones and J. Henderson 1985 *Vibration Damping*. New York: John Wiley.
27. T. Kailath 1980 *Linear Systems*. Englewood Cliffs, New Jersey: Prentice-Hall.
28. H. Kwakernaak and R. Sivan 1972 *Linear Optimal Control Systems*. New York: John Wiley.
29. R. F. Stengel 1986 *Stochastic Optimal Control—Theory and Application*. New York: John Wiley.
30. W. H. Liao and K. W. Wang 1996 *IOP Journal of Smart Materials and Structures*, **5,** 638–648. A new active constrained layer configuration with enhanced boundary actions.
31. W. H. Liao and K. W. Wang 1997 *Proceedings of DETC'97 ASME Design Engineering Technical Conference*, DETC97VIB-3778 and 4172, Sacramento, California. Characteristics of Enhanced Active Constrained Layer Damping Treatments with Edge Elements, Part 1: Finite Element Model and Experimental Validation, and Part 2: System Analysis.

APPENDIX: NOMENCLATURE

$\mathbf{A}$	open-loop system matrix
A_b, A_c, A_s	cross sectional area of beam, piezoelectric layer, and VEM, respectively
$\mathbf{A}_{cl}$	closed-loop system matrix
$\mathbf{B}$	control matrix
$\hat{\mathbf{B}}$	disturbance matrix
b	width for beam, piezoelectric layer, and VEM
$\mathbf{C}$	damping matrix
$\mathbf{C}_b$	Rayleigh damping matrix
$\mathbf{C}_o$	output matrix
C_{11}^D	Young's modulus of piezoelectric materials with open circuit
D	electrical displacement
E	electric field
E_b	Young's modulus of beam
E[]	expectation operator
$\mathbf{f}_c$	control vector
$\mathbf{f}_d$	disturbance force vector
G	relaxation function of VEM
G^*	complex modulus of VEM
G_1	shear modulus of VEM
h_{31}	piezoelectric constant
I_a	index of active action authority
I_{ap}	effectiveness index of active–passive hybrid actions
I_b, I_c	moment of inertia of beam and piezoelectric layer
I_p	index for passive damping ability
J_1	index of vibration control performance
J_2	index of required control effort
J_s	cost rate
$\mathbf{K}$	stiffness matrix
$\mathbf{K}_c$	control gains
L	beam length
$\mathbf{M}$	mass matrix
$\mathbf{Q}$	weighting matrix on output
$\mathbf{q}$	displacement vector
$\mathbf{R}$	weighting matrix on control input
t	time
t_b, t_c, t_s	thickness of beam, piezoelectric layer, and VEM, respectively
$\mathbf{u}$	control input
$\mathbf{u}_d$	disturbance input vector
u_b, u_c, u_s	axial displacement of beam, piezoelectric layer, and VEM, respectively
V	applied voltage
$\mathbf{W}$	output covariance matrix
w	beam transverse displacement
x	position co-ordinate along beam length
$\mathbf{x}$	state vector
x_1	left end of ACL
x_2	right end of ACL
$\mathbf{y}$	output vector
α	weighting on GHM dissipation co-ordinate
β	shear strain of VEM
β_{33}^s	dielectric constant of piezoelectric materials
ε	mechanical strain of piezoelectric materials
$\hat{\zeta}$	damping factor in GHM dissipation co-ordinate
η	material loss factor of VEM
κ	final value of $G(t)$
ρ_b, ρ_c, ρ_s	mass density of beam, piezoelectric layer, and VEM, respectively
τ	mechanical stress
ψ	rotational angle in VEM
$\hat{\omega}$	natural frequency in GHM dissipation co-ordinate